J. Space Weather Space Clim., **5**, A38 (2015)
DOI: 10.1051/swsc/2015039

RESEARCH ARTICLE OPEN ACCESS

Matroshka DOSTEL measurements onboard the International Space Station (ISS)

Johannes Labrenz[1,*], Soenke Burmeister[1], Thomas Berger[2], Bernd Heber[1], and Guenther Reitz[2]

[1] Christian-Albrechts-Universität zu Kiel, Christian-Albrechts-Platz, 24118 Kiel, Germany
[*]Corresponding author: labrenz@physik.uni-kiel.de
[2] German Aerospace Center (DLR), Institute of Aerospace Medicine, Linder Hoehe, 51147 Cologne, Germany

Received 1 April 2015 / Accepted 8 November 2015

ABSTRACT

This paper presents the absorbed dose and dose equivalent rate measurements achieved with the DOSimetry TElescope (DOSTEL) during the two Matroshka (MTR) experiment campaigns in 2004/2005 (MTR-1) and 2007/2008 (MTR-2B). The comparison between the inside (MTR-2B) and outside (MTR-1) mission has shown that the shielding thickness provided by the International Space Station (ISS) spacecraft hull has a minor effect on the radiation exposure caused by Galactic Cosmic Rays (GCR). The exposure varies with the solar modulation of the GCR, too. Particles from Earth's radiation belts are effectively shielded by the spacecraft hull, and thus the contribution to the radiation exposure is lower for the inside measurement during MTR-2B. While the MTR-DOSTEL absorbed dose rate shows a good agreement with passive detectors of the MTR experiment for the MTR-2B mission phase, the MTR-1 absorbed dose rates from MTR-DOSTEL measurements are much lower than those obtained by a nearby passive detector. Observed discrepancies between the MTR-DOSTEL measurements and the passive detectors located nearby could be explained by the additional exposure to an enhanced flux of electrons trapped between L-parameter 2.5 and 3.5 caused by solar storms in July 2004.

Key words. Galactic cosmic rays – Radiation belts – Dosimetry – International Space Station – Matroshka

1. Introduction

The radiation environment in Low Earth Orbit (LEO) is completely different in comparison to the one on ground. The environment is populated by high-energy galactic cosmic rays (GCR) and during enhanced solar activity by solar energetic particles (SEP). In addition, there are charged particles trapped in Earth's magnetic field (radiation belts), which are able to reach International Space Station (ISS) altitudes in the South Atlantic Anomaly (SAA) and in polar regions (Xapsos et al. 2013). The complex structure of the radiation environment is difficult to simulate comprehensively on the ground. For studies of the exposure levels of human beings, human phantoms are used in order to provide dose-versus-depth distributions to estimate organ doses. The European Space Agency (ESA) MATROSHKA (MTR) experiment under the project lead of DLR aims to measure the radiation exposure to an astronaut as accurately as possible. For this purpose a phantom of an upper human torso equipped with radiation measurement devices was brought to the ISS. A detailed description of the MTR experiment is given in Dettmann et al. (2007). The radiation measurement devices of MTR can be grouped into passive and active detectors. Descriptions and results of the passive detectors can be found in Reitz & Berger (2006); Reitz et al. (2009); Zhou et al. (2010); Berger et al. (2013), and will not be further evaluated in this work. The active instrumentation of MTR consists of a Tissue Equivalent Proportional Counter (TEPC) provided by NASA, four Silicon Scintillator Devices (SSDs), and a Dosimetry Telescope (DOSTEL). The SSDs and the MTR-DOSTEL were built at the Christian-Albrechts University Kiel (CAU).

In this work data obtained with MTR-DOSTEL will be presented. One advantage of an active instrument, like MTR-DOSTEL, is the provision of time-resolved data and thus a spatial correlation of the data with the ISS orbit. That allows to separate the different contributions to the total radiation exposure of GCR, SEP, and the trapped component. Time resolution also provides information on temporal changes of the radiation field. It is known that the GCR intensity varies with the solar activity and that solar particle events can contribute to the radiation exposure in LEO. An elevated radiation exposure due to solar particles was measured by DOSTEL as part of the DOSMAP experiment in April 2001 (Reitz et al. 2005). In the last decade temporal changes of particle fluxes were observed in the radiation belt due to geomagnetic storms (e.g. the Halloween storm 2003, Baker et al. 2004). Enhanced particle fluxes in the outer radiation belt and slot region can extend down to ISS altitudes (Shurshakov et al. 1996) and may contribute significantly to the radiation exposure. The MTR-DOSTEL has shown that in autumn 2004 a high amount of electrons was trapped between $L = 2.5$ and 3.5 and reached down to ISS altitudes south of South Africa. MTR-DOSTEL data from September and October 2004 was used to estimate the additional radiation exposure due to this enhanced particle flux (EPF).

2. Instrumentation

DOSTEL is a particle telescope built of silicon semiconductor detectors. It is designed to operate in Low Earth Orbit (LEO). The first DOSTEL was flown as part of the

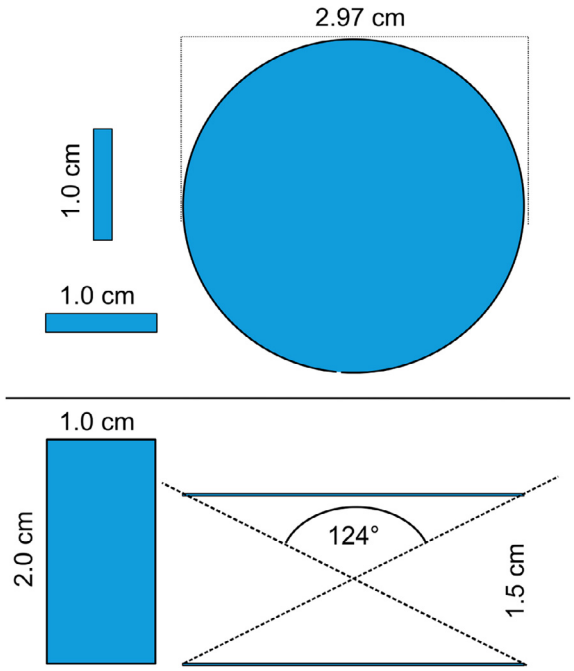

Fig. 1. Sketch of the MTR-DOSTEL detector head. The upper sketch shows the view from top and the lower sketch a side view of the detectors. The two PIPS detectors form a telescope with an opening angle of 124°. The Hamamatsu PIN diodes are mounted perpendicular to each other and to the telescope.

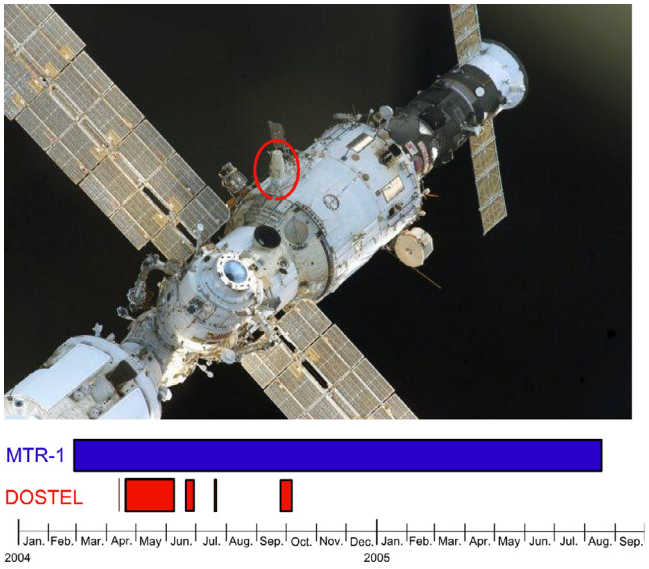

Fig. 2. Photograph of MTR and sketch of data coverage of MTR-DOSTEL during the MTR-1 mission phase.

Dosimetric Mapping inside Biorack on the Shuttle-to-MIR mission STS 76 in March 1996 (Reitz et al. 1999; Beaujean et al. 1999a, 1999c). Since then, different DOSTEL units were used for dose measurements on aircraft (Beaujean et al. 1999b), the Russian MIR station (Badhwar et al. 2002; Beaujean et al. 2002), and on the ISS as part of the DOSMAP experiment (Reitz et al. 2005) as well as the MTR experiment (2004, 2008) and the DOSIS and DOSIS 3D experiments (since 2009). The MTR-DOSTEL consists of a particle telescope made of two Passivated Implanted Planar Silicon (PIPS) detectors and two PIN diodes perpendicular to each other and the telescope (see Fig. 1). The specification of the detectors is shown in Table 1. DOSTEL measures the amount of energy deposited in the detectors by ionizing radiation (mainly charged particles). Neutrons can only be detected indirectly via elastic scattering or compound nuclear reaction, and thus the dose deposited by neutral particles is underestimated by DOSTEL. The energy loss information is then stored in 8-bit energy deposition spectra (256 channels), which are integrated over one half of the ISS orbit. During crossings of the inner radiation belt in the region of the South Atlantic Anomaly (SAA), DOSTEL switches to SAA-mode via a threshold of the slope of the count rate. It exits SAA-mode if the count rates fall below an exit threshold. In SAA-mode the data is stored in separate energy deposition spectra. The telescope detectors measure alternating in coincidence and single mode. In coincidence mode only particles hitting both telescope detectors contribute to the energy deposition spectra. In single mode no coincidence is required and all particles are stored in the energy deposition spectra. The PIN diodes always measure in single mode. The MTR-DOSTEL in addition provides a count rate with 100 s time resolution (20 s during SAA-mode). All particles hitting one of the four MTR-DOSTEL detectors contribute to this count rate.

The active instrumentation of MTR was used during two measurement campaigns of the experiment. During the MTR-1 mission the experiment was mounted outside the Zvezda module of the International Space Station (ISS) from February 2004 to August 2005 (see Fig. 2). From October 2007 to November 2008 the second mission phase with use of active instrumentation (MTR-2B) took place inside the Zvezda module (see Fig. 3). The MTR-DOSTEL data is not covering the whole mission times, due to interface problems with the platform main data processing unit. The whole mission times and the data coverage of MTR-DOSTEL during MTR-1 are shown in Figure 2. The mission lasted from February 26th, 2004 to August 18th, 2005. MTR-DOSTEL recorded data on April 13th, from April 20th until June 9th, from June 19th to June 30th, from July 19th to 22nd, and from September 24th to October 8th, 2004. Additionally there are

Table 1. Specification of the four DOSTEL detectors. The thickness (column 2), area (column 3), mass (column 5), and energy deposition ranges (column 5) are shown. For the telescope detectors these energy ranges can be converted to LET in water.

Detector	Thickness/(μm)	Area/(cm^2)	Mass/(g)	dE range/(keV) LET range/(keV μm^{-1} in water)
Upper tele. detector	154	6.93	0.249	dE_i = [28.7,. . ., 22612] LET$_i$ = [0.084,. . ., 66.3]
Lower tele. detector	315	6.93	0.509	dE_i = [42.5,. . ., 51248] LET$_i$ = [0.061,. . ., 73.5]
Pin diodes	300	2.31	0.161	dE_i = [44.4,. . ., 56292] no pathlength limitation

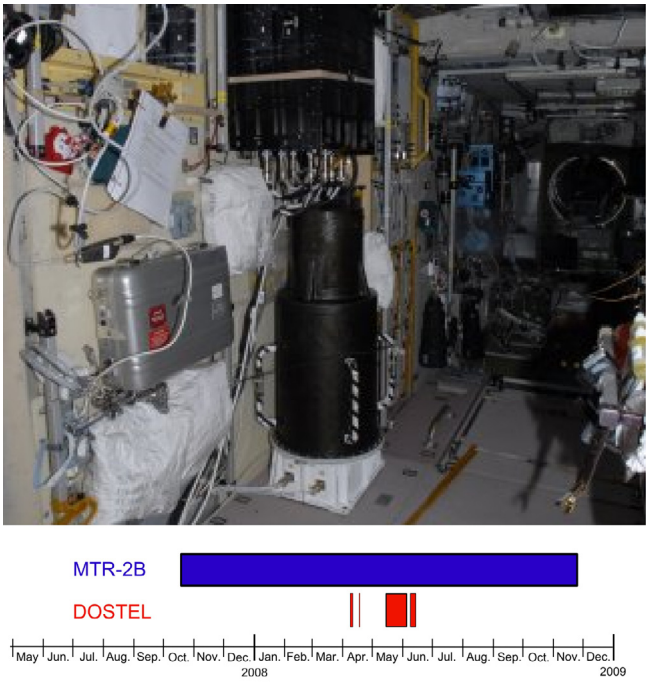

Fig. 3. Photograph of MTR and sketch of data coverage of MTR-DOSTEL during MTR-2B mission phase.

smaller data gaps between April 20th and June 30th, as well as between September 24th and October 8th. The total measurement time of MTR-DOSTEL during MTR-1 was 71 days. The time line of the MTR-2B mission is shown in Figure 3. The exposure lasted from October 18th, 2007 until November 25th, 2008. During this time the passive detectors of MTR were exposed to the radiation field inside the ISS. The MTR-DOSTEL has recorded data from April 8th to April 11th, April 17th to 18th, May 14th to June 6th, and June 9th until June 15th. Due to additional data gaps the total measurement time of MTR-DOSTEL during MTR-2B was 31 days. The incomplete data coverage of MTR-DOSTEL has to be considered when comparing MTR-DOSTEL results with results of the passive instrumentation of MTR. The passive detectors deliver mission-integrated data, while MTR-DOSTEL data are available only for a fraction of the mission time.

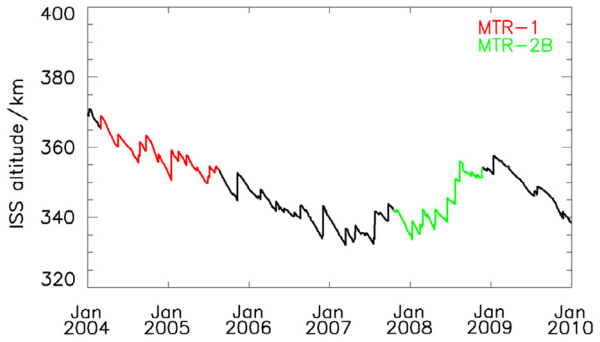

Fig. 5. The altitude of the ISS from 2004 until 2010. The MTR mission phases are shown in color code (MTR-1 red and MTR-2B green).

As already stated the radiation environment on ISS is affected by the solar cycle and the altitude of the ISS. Figure 4 shows the count rate of the NM64 Jungfraujoch neutron monitor (NM) to demonstrate the influence of the solar cycle on the GCR flux for the MTR-1 (left panel) and MTR-2B mission (right panel). During the MTR-2B mission the sun was closer to solar minimum, as seen in an increase of the NM count rate (and GCR flux) in respect to the MTR-1 mission. Figure 4 shows in addition the K_p index in color code. It can be seen that during the MTR-1 mission the magnetic field of Earth was much more disturbed (solar maximum) than during the MTR-2B mission. The altitude of the ISS from January 2004 until January 2010 is shown in Figure 5. During the MTR-1 mission (red) the altitude of the station decreased. During the MTR-2B mission (green) the altitude of the station increased in summer 2008.

3. Materials and methods

The single mode energy deposition spectra measured with MTR-DOSTEL are used to calculate the absorbed dose D. D is the amount of energy per mass deposited in an absorber. The calculation is shown in Eq. (1). The number of particles per energy channel times the energy of the channel are summed up over all channels and divided by the mass of the detector. The energy is given in joule and the mass in kg. The resulting quantity is called gray ($1\,\mathrm{Gy} = 1\,\frac{\mathrm{J}}{\mathrm{kg}}$).

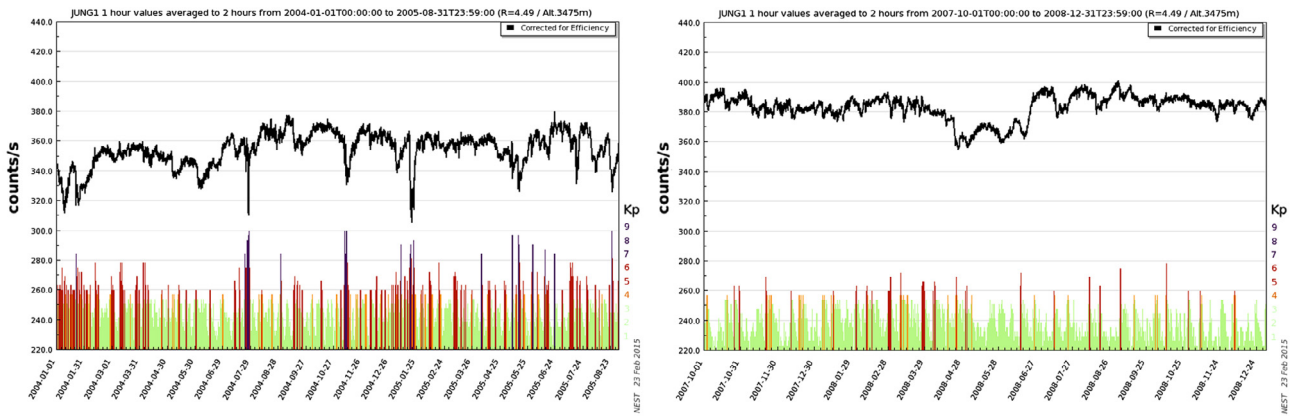

Fig. 4. The count rate of the NM64 Jungfraujoch neutron monitor (black line) as measure for the CR flux and the planetary K_p index as measure for the disturbances in Earth's magnetic field are shown for the MTR-1 (left) and MTR-2B mission phase (right), plots were created using nest2.nmdb.eu.

$$D_{\mathrm{Si}} = \sum_i \frac{dE_i \times N_i}{m} = \sum_i \frac{dE_i \times N_i}{V \times \rho} = \sum_i \frac{dE_i \times N_i}{A \times d \times \rho}. \quad (1)$$

In radiation biology the absorbed dose is usually given as absorbed dose in water. In this work the absorbed dose in silicon D_{Si} is converted to absorbed dose in water by using a constant conversion factor of 1.23 (see Eq. (2)). The factor of 1.23 results from different stopping powers (ICRU 1984) for electrons and protons in silicon and water. Because an identification of the particle species is not possible with DOSTEL, an average over all LETs for protons and electrons is used. The calculation of this value is described in Beaujean et al. (1999b). A constant conversion factor is commonly used in space dosimetry (see Doke et al. 2001; Pazmandi & Deme 2003).

$$D = D_{\mathrm{Si}} \times F_{\mathrm{Si}\rightarrow water} = D_{\mathrm{Si}} \times 1.23. \quad (2)$$

In this work we use the quantity dose equivalent (H) to calculate the radiation exposure onboard the ISS. H is the product of the absorbed dose D and the quality factor Q. Q characterizes the biological effectiveness of a radiation and is defined as a function of the unrestricted linear energy transfer often denoted as LET (ICRP, 2007). The LET is the amount of energy deposited by ionizing radiation along its pathlength (see Eq. (3)).

$$\mathrm{LET}_i = \frac{\mathrm{d}E_i}{\mathrm{d}l} \times F_{\mathrm{Si}\rightarrow water} \times \frac{\rho_{\mathrm{H_2O}}}{\rho_{\mathrm{Si}}} = \frac{\mathrm{d}E_i}{\mathrm{d}l} \times 1.23 \times \frac{1}{2.33}. \quad (3)$$

For the calculation of the dose equivalent, only energy deposition spectra recorded in coincidence mode are used to calculate a mean quality factor $\langle Q \rangle$. The ionizing radiation measured in this MTR-DOSTEL mode had to penetrate both telescope detectors and thus the pathlength in the detectors is limited. With a mean particle pathlength in the detectors of $\frac{1}{\cos(\langle\theta\rangle)}$, where $\langle\theta\rangle$ is the mean angle of incidence for an isotropic particle flux, the LET of each energy channel can be determined. To calculate the dose equivalent H_{coinc} of the particles penetrating both detectors, the absorbed dose of each energy channel in the energy deposition spectra $D_{\mathrm{coinc},i}$ is weighted with the corresponding LET-dependent quality factor Q_i. The mean quality factor is calculated by dividing the dose equivalent H_{coinc} by the absorbed dose D_{coinc} for particles complying with the coincidence condition.

$$\langle Q \rangle = \frac{H_{\mathrm{coinc}}}{D_{\mathrm{coinc}}} = \frac{\sum_i D_{\mathrm{coinc},i} \times Q_i}{\sum_i D_{\mathrm{coinc},i}}. \quad (4)$$

This ratio can also be assumed as the ratio between the dose equivalent and absorbed dose for all particles measured with MTR-DOSTEL. Thus this factor can be used to scale the absorbed dose D deposited from all particles hitting a detector to the dose equivalent H deposited by all particles (see Eq. (5)).

$$H = D \times \langle Q \rangle. \quad (5)$$

The calculated mean quality factor $\langle Q \rangle$ was used to convert the absorbed dose in water D into dose equivalent H for all four detectors of MTR-DOSTEL. The dose values presented in this work are mean values averaged over 53 days for MTR-1 and 31 days for MTR-2B. For such long time periods the number of entries in the energy deposition spectra is high and the statistical error is negligible ($\ll$1%). The constant conversion factor used in this work is 1.23. In the literature, different values of a mean factor for converting energy loss in silicon to energy loss in water can be found. A conversion factor of 1.193 (assuming only relativistic particles) was used in Doke et al. (2001), whereas 1.23 was calculated (for protons) in Pazmandi & Deme (2003). In both works the uncertainty for these values was estimated to be around 5%. This uncertainty is assumed for this work, too. Because the absorbed dose (in water), the LET, and the dose equivalent depend on the conversion factor, the 5% uncertainty in the conversion of deposited energy in silicon to deposited energy in water results in a systematic uncertainty of 5% for all dose values and mean quality factors presented in this work.

4. Data analysis

4.1. MTR-2B dose values

In this section the results of the dose values obtained with MTR-DOSTEL will be shown and compared to results of other instruments on ISS. The dose values for the MTR-2B mission, calculated as described in the previous section, are shown in Table 2. The dominating contribution to the total absorbed dose results from GCR particles (70%). Due to the higher biological effectiveness of GCR particles ($\langle Q \rangle$ = 2.8) compared to trapped particles ($\langle Q \rangle$ = 1.6) the contribution to the dose equivalent rate is even higher (80%). The daily dose rates of trapped particles are accumulated mainly during the crossings of the inner radiation belt which takes ~50 min per day.

The MTR-DOSTEL measured a mean absorbed dose rate of about 160 μGy day^{-1} for the time between April and June 2008. The contribution from GCR particles was 115 μGy day^{-1} and 45 μGy day^{-1} result from particles of the inner radiation belt in the SAA region (SAA). The four DB-8 units located in the Zvezda module have measured an absorbed dose rate induced by GCR particles of 100 μGy day^{-1} (Lishnevskii et al. 2010). The absorbed dose rate from trapped particles differs between the four DB-8 units because of the strong dependence on the local shielding of the detectors. The unit closest to MTR showed the lowest dose rate of 60 μGy day^{-1}. During the MTR-2B mission the MTR-DOSTEL had some problems with noise in one of the detectors. This noise only had a minor influence on the energy deposition spectra of the noisy detector. The MTR-DOSTEL count rate is the number of particles hitting any of the detectors. Due to this the noisy detector influenced the count rate. This led to the problem, that the MTR-DOSTEL switched randomly to SAA-mode. Therefore, the separation of SAA and GCR component for the MTR-2B mission data was done afterward by using the shape of the recorded energy deposition spectra. This separation is not very accurate. Especially energy deposition spectra containing only short times of inner radiation belt crossing can be counted as GCR spectra. This led to a higher GCR and lower trapped particle dose rate and would explain the small differences in the absorbed dose rate between MTR-DOSTEL and the DB-8 units for the two contributions, while the total absorbed dose rate is in very good agreement. Passive detectors do not allow time-resolved data and show the mean dose rates integrated over the whole MTR-2B mission time (from October 2007 to November 2008). The measurements referred to in this work were obtained with ^{7}LiF:Mg, Ti (TLD-700) thermoluminescence

Table 2. Absorbed dose rate $\dot{D}$ and the dose equivalent rate $\dot{H}$ for the GCR and the SAA component as well as the sum of both (total) for the time period from April 8th to June 15th 2008 during MTR-2B mission phase.

MTR-2B	$\dot{D}$/(μGy day^{-1})	$\dot{H}$/(μSv day^{-1})	$\langle Q \rangle$
GCR	115.6	309.8	2.79
SAA	45.8	72.4	1.58
Total	161.4	382.2	2.37

Table 3. Absorbed dose rate $\dot{D}$ and the dose equivalent rate $\dot{H}$ for the GCR and the SAA component as well as the sum of both (total) for the time period from April 13th to June 30th 2004 during the MTR-1 mission phase.

MTR-1	$\dot{D}$/(μGy day^{-1})	$\dot{H}$/(μSv day^{-1})	$\langle Q \rangle$
GCR	77.6	245.5	3.16
SAA	296.1	367.1	1.24
Total	373.7	612.3	1.64

detectors. The detectors are mainly sensitive to charged particles, which allows a comparison of the measured dose values with MTR-DOSTEL results. The energy range of TLD-700 has the same lower border as the MTR-DOSTEL, but the TLD detectors are not very sensitive to LETs above 10 keV μm^{-1} (Berger & Hajek 2008). For the GCR contribution, the TLDs should detect 90% of the absorbed dose measured with MTR-DOSTEL. Most of the particles of the trapped component deposit less than 10 keV μm^{-1} in the detectors, and thus the differences between MTR-DOSTEL and the TLD detectors are negligible for the trapped component. The total absorbed dose measured with TLD-700 should be slightly lower than the MTR-DOSTEL results. TLDs located close to MTR-DOSTEL have measured an absorbed dose rate of 189 μGy day^{-1} (Berger et al. 2013). The higher mean dose rate measured by the passive detectors can be explained by an altitude increase, and thus higher flux of trapped particles (see Fig. 5). The decreasing solar activity resulting in a slightly higher GCR flux (see Fig. 4) toward the end of the mission plays a minor role for the differences.

4.2. MTR-1 dose values

The dose rates measured outside the ISS during the MTR-1 mission are shown in Table 3 (only for the time frame up to end of July 2004). A strongly increased contribution from trapped particles can be seen in comparison to the inside measurement (MTR-2B). The trapped particles contribute ~80% to the total absorbed dose rate. The GCR particles have a higher biological effectiveness ($\langle Q \rangle_{GCR}$ = 3.16) compared to trapped particles ($\langle Q \rangle_{SAA}$ = 1.24). Therefore the trapped component is not that dominant in the dose equivalent rate, but still contributes ~60% to its total value. A comparison of the absorbed dose rates measured by MTR-DOSTEL for the inside (bottom) and outside (top) measurement campaigns is shown in Figure 6 (there shown data from September to October 2004 is discussed later in Sect. 4.3). The missing shielding of the ISS hull for MTR-1 led to an increase of the dose obtained from trapped particles. Especially electrons (e.g. from the edges of the outer radiation belt) are effectively shielded by the spacecraft hull and thus only contribute to the absorbed dose during the outside measurement. The lower mean quality

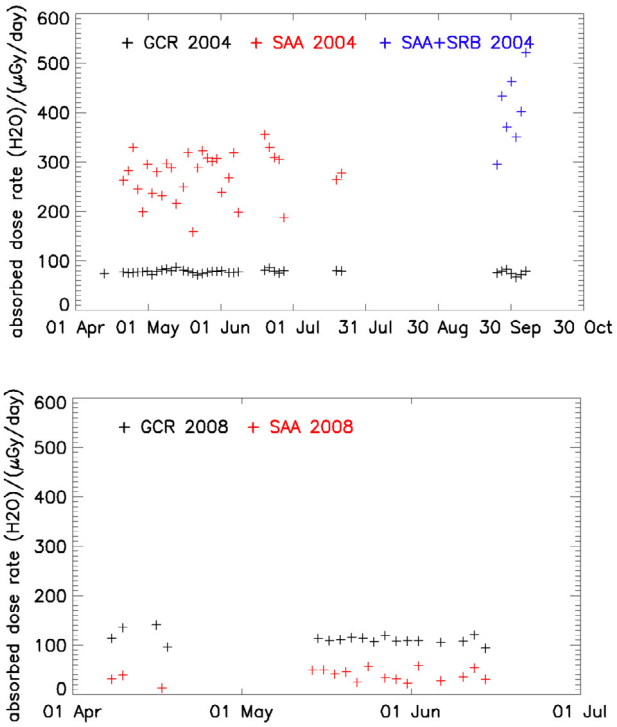

Fig. 6. Absorbed dose rate measured with MTR-DOSTEL during MTR-1 (top) and MTR-2B (bottom) mission phase. The dose rates are averaged over a two-day interval.

factor for trapped particles outside the ISS in addition indicates a greater influence from the electrons on the mean dose. The GCR-induced absorbed dose during the outside exposure is smaller than during the inside measurement. This can be explained by changes in the solar activity and shielding conditions. The count rate of the Jungfraujoch neutron monitor increased between MTR-1 and MTR-2B by about ~10% (see Fig. 4). The absorbed dose measured by MTR-DOSTEL increased from 78 to 100 μGy day^{-1} (28%). This indicates that ~20% (15 μGy day^{-1}) of the absorbed dose increase from MTR-1 to MTR-2B results from differences in the shielding conditions. GCR interactions in the spacecraft structure are producing lower-energy protons, neutrons, etc. Especially secondary lower-energy protons from GCR nuclear collisions are affecting the dose measured with MTR-DOSTEL. Thicker shielding leads to a higher amount of low-energy protons, and thus to a higher observed absorbed dose rate. Calculations by Matthiä et al. (2013) indicate that for the GCR contribution in 2009 an absorbed dose rate of 100 μGy day^{-1} is expected behind a shielding of ~35 g cm^{-2} Al (MTR-2B), whereas 85 μGy day^{-1} corresponds to a shielding of ~20 g cm^{-2} Al (MTR-1). This means the outside measurement is not comparable to a measurement with just a detector in LEO. In the ISS structure, the MTR phantom was attached to, secondary particles are produced and add to the measured absorbed dose rate.

MATROSHKA was the only radiation experiment outside the ISS during the MTR-1 mission. Therefore a comparison can only be made between MTR-DOSTEL and the passive detectors of the experiment. As for the MTR-2B mission phase the MTR-DOSTEL data does not cover the whole mission time (here shown from April 13th 2004 to June 30th 2004), while the passive detectors had accumulated the dose over the whole mission time from February 26th 2004 to August 18th 2005.

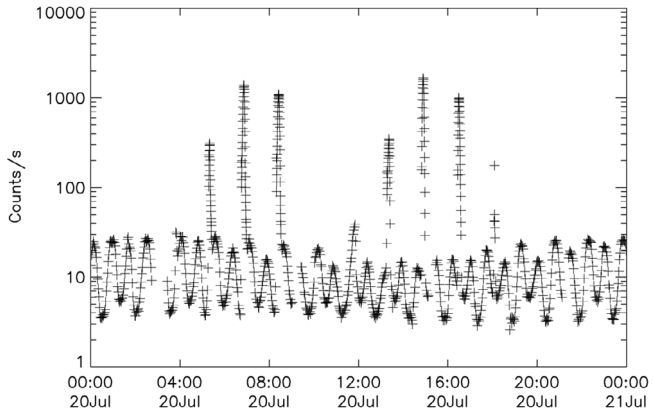

Fig. 7. Time profile of count rates measured by MTR-DOSTEL on July 20th 2004. The dependence on the geomagnetic cutoff rigidity can be seen in the 45 min modulation of the data. The spikes in the count rate result from crossings of the inner radiation belt in the region of the SAA.

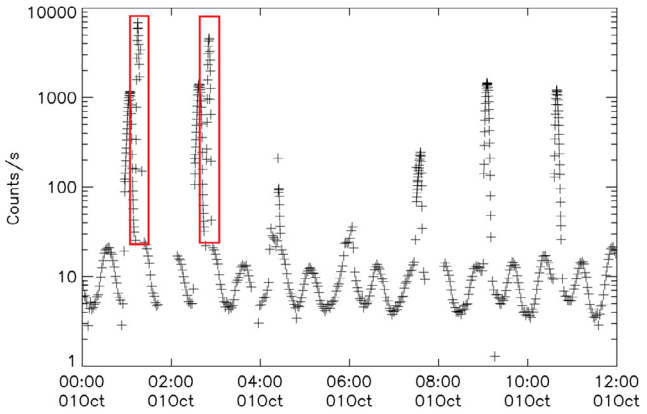

Fig. 8. Time profile of count rates measured by MTR-DOSTEL during October 1st 2004. Directly after the increased count rate due to inner radiation belt crossing at 01:00 am and 02:30 am, two additional spikes with count rates up to 6000 particles per second can be seen (marked with the red boxes).

The absorbed dose for the skin of the MTR phantom of 944 μGy day^{-1} (Reitz et al. 2009) is more than two times higher than the results obtained with MTR-DOSTEL 373.7 μGy day^{-1}. The shielding of the MTR-DOSTEL is slightly higher in respect to the skin detectors. This should result in a lower absorbed dose rate measured by MTR-DOSTEL. But even the absorbed dose of 540 μGy day^{-1} measured with thermoluminescent detectors (TLDs) next to MTR-DOSTEL with similar shielding conditions is higher than the MTR-DOSTEL results (Berger et al. 2013). The huge differences in MTR-DOSTEL absorbed dose rates and the skin measurements can be explained by different shielding thicknesses which in the case of electrons can lead to a large change in the measured absorbed doses. The K_p index shown in Figure 4 shows that during the MTR-1 mission Earth's magnetic field was much stronger and often disturbed than during MTR-2B. The difference of MTR-DOSTEL measurements and the nearby passive detectors can be well explained by the additional contribution to the absorbed dose by particles that formed an additional radiation belt and outer electron belt enhancements as explained in the following Section 4.3. It is important to emphasize that a change in mean shielding thickness can cause strong effects, especially since we have a major contribution by electrons to the dose.

4.3. Variation of the radiation field in LEO

Figure 7 shows as an example a typical count rate profile of the MTR-DOSTEL, taken on July 20th 2004. The count rates of the GCR particles (3–20 counts per second) show an oscillating wave like time dependence. This results from the count rate dependence on the geomagnetic cutoff rigidity. At locations with lower cutoff rigidity (high geomagnetic latitudes) more GCR particles reach ISS altitudes and thus the MTR-DOSTEL count rate is higher compared to locations with higher cutoff rigidities (geomagnetic equator). The ISS orbits the Earth in about 90 min. During one orbit the ISS crosses high latitudes (North), the geomagnetic equator, high latitudes (South), and again the geomagnetic equator. This leads to an oscillating wave like structure with maxima (and minima) every 45 min. The spikes in the count rate profile (up to 1000 counts per second) are related to the region of the South Atlantic Anomaly (SAA) where the ISS crosses the inner radiation belt. The ISS crosses the SAA region 3–5 times per day from North to South (descending) and 3–5 times from South to North (ascending). The time between the crossings in one direction (descending or ascending) is ~90 min (as can be seen in Fig. 7). As shown in the time line of the MTR-1 mission phase (Fig. 2) the MTR-DOSTEL was operating in September and October 2004 too. As an example, Figure 8 shows the count rate profile for the first 12 h of October 1st 2004. The GCR count rate shows the same behavior as in Figure 7. The difference to the count rate profile of July 20th are additional spikes (up to 6000 counts per second) directly after the descending crossings of the SAA region. These spikes are marked with red boxes in Figure 8.

In order to investigate these additional spikes in more detail, we used the ISS orbit data to visualize the geographic distribution of the MTR-DOSTEL count rates. The situation in May 2004 is presented in the top panel of Figure 9. The crossings of the inner radiation belt in the region of the SAA can be seen, as well as the GCR count rate dependence on the geomagnetic latitude. At the highest geomagnetic latitudes increased count rates can be seen. They result from crossings of the edges of the outer radiation belt. As already seen in Figure 8 the situation was different in October 2004. This is visualized in the bottom panel in Figure 9. The geographic count rate distribution shows that the additional count rate spikes belong to a localized region south of South Africa. It can further be seen that the count rates at high geomagnetic latitudes are as well increased. The edges of the outer radiation belt reached down to ISS altitudes more often than in May 2004. Figure 10 shows the same count rate data, as presented in Figure 9, in dependence on the McIlwain L-parameter (McIlwain 1961). For this visualization an approach from Shea et al. (1987), which allows the calculation of the L-parameter from vertical geomagnetic cutoff rigidity, was used. The count rate shows a strong dependence on the L-parameter. The GCR count rate (black) is the highest for highest L-values. At a constant altitude the highest L-parameter is reached at highest geomagnetic latitudes. The upper panel presents the data of May 2004. The trapped particle component (red) shows a distribution between L-values of 1.2 and 2.0. These are the typical L-shells of the inner radiation belt (Durante & Cucinotta 2011). The depletion between $L = 2$ and 3 forms the slot region. The few enhanced count rates in the L-region between

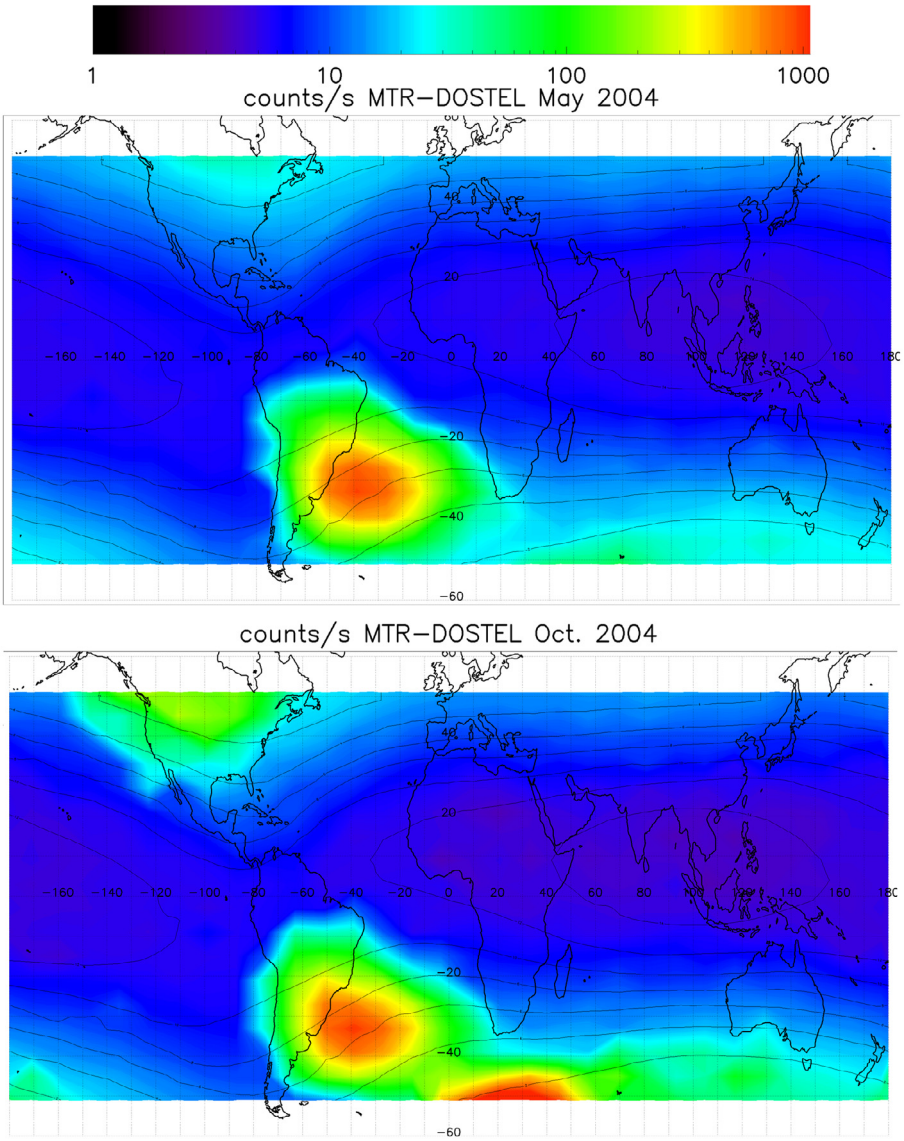

Fig. 9. MTR-DOSTEL geographical count rate distribution for May 2004 (top) and October 2004 (bottom) during the MTR-1 mission phase.

3 and 5 belong to crossings of the edges of the outer radiation belt. For the September and October data the count rate dependence on the *L*-parameter (bottom) shows that the *L*-parameter interval of the additional spikes reaches from ~2.5 to 3.5. The trapped particles reach down to the Slot Region which under normal conditions is characterized by a very low flux of trapped particles (Lyons & Thorne 1973; Korth & Vampola 1994).

Radiation belt observations are performed by instruments especially designed for this purpose. During the outside exposure of MTR experiments for radiation belt observations were conducted in space, too. One of them was the Solar Anomalous and Magnetospheric Particle Explorer (SAMPEX; Baker et al. 1993). SAMPEX had a polar orbit around the Earth and was able to measure charged particles at different *L*-parameters. A time profile of *L*-parameter spectra of electrons with energies between 3.5 MeV and 16 MeV is shown in Figure 11. The region between $L = 2$ and 3 shows a low electron intensity until DOY 209 (July 27th, 2004). After that, a strong increase of relativistic electrons at *L*-parameters between 2.5 and 4 was observed. The intensity of these particles decayed in time but was observed until DOY 310. The filling of Earth's magnetic field around July 27th is associated with three geomagnetic storms driven by interplanetary Coronal Mass Ejections (CME) with Disturbance Storm Time (DST) indices of −101, −148, and −197 nT (Zhang et al. 2007). The last of these storms is characterized by high solar wind speeds combined with a southward interplanetary magnetic field component. A detailed description of the three geomagnetic storms around July 27th is given in Kuznetsov et al. (2009).

Unfortunately there is no MTR-DOSTEL data available for the time period between July 22nd and September 24th. But the MTR-DOSTEL data from September 24th to October 8th were obtained during the presence of the enhanced particle flux (EPF). An LET spectrum of these particles and the inner radiation belt protons (September 2004) is shown as an example in the lower panel of Figure 12 in black. In comparison an LET spectrum of only inner radiation belt crossing (May 2004) with comparable orbital parameters is shown in red. The EPF particles show LETs below 2 keV μm^{-1} with a maximum at an LET of 0.15 keV μm^{-1}. The energy depositions of the EPF particles show that most of them are relativistic particles. Relativistic particles trapped in Earth's magnetic field have to

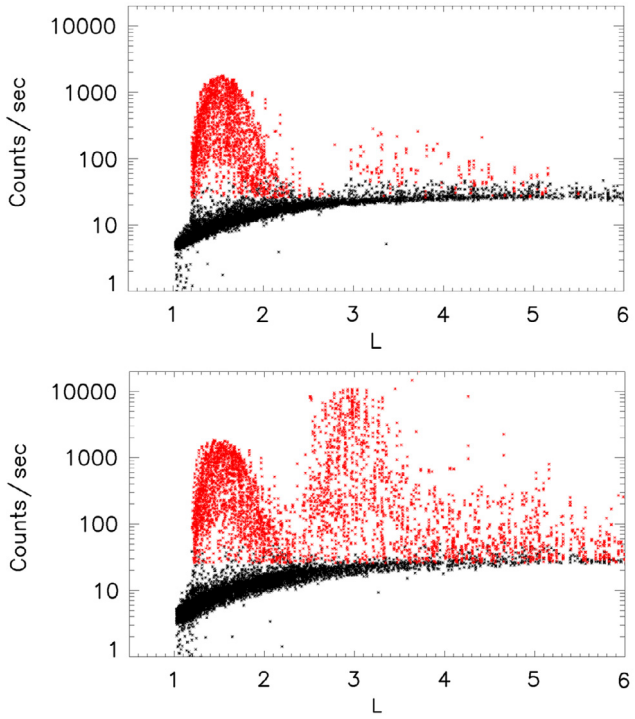

Fig. 10. L-parameter count rate distribution for May 2004 (top) and September/October 2004 (bottom) during the MTR-1 mission phase. Besides the crossing of the inner radiation belt in the SAA region ($1 < L < 2$), the September/October data shows an additional region with enhanced count rates between $2.5 < L < 3.5$.

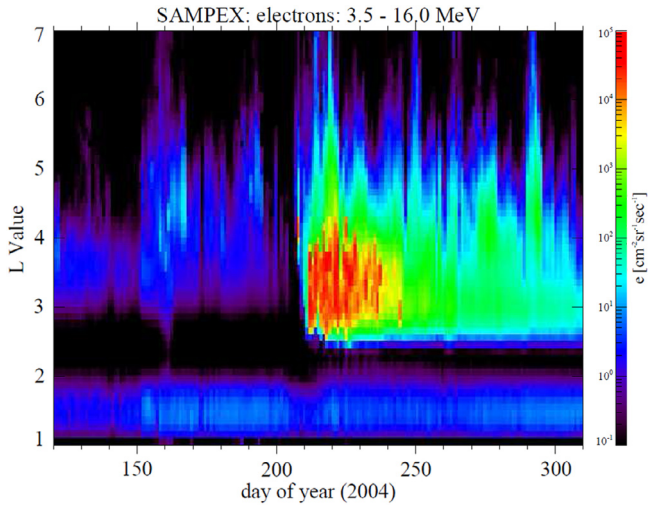

Fig. 11. Flux of electrons in the energy range of 3.5–16 MeV measured by the SAMPEX satellite. Earth's magnetic field was filled with relativistic electrons at DOY 209 (July 27th) in 2004. Picture taken in July 2010 from SAMPEX Data Center (http://lasp.colorado.edu/app/sampex/data-viewer/).

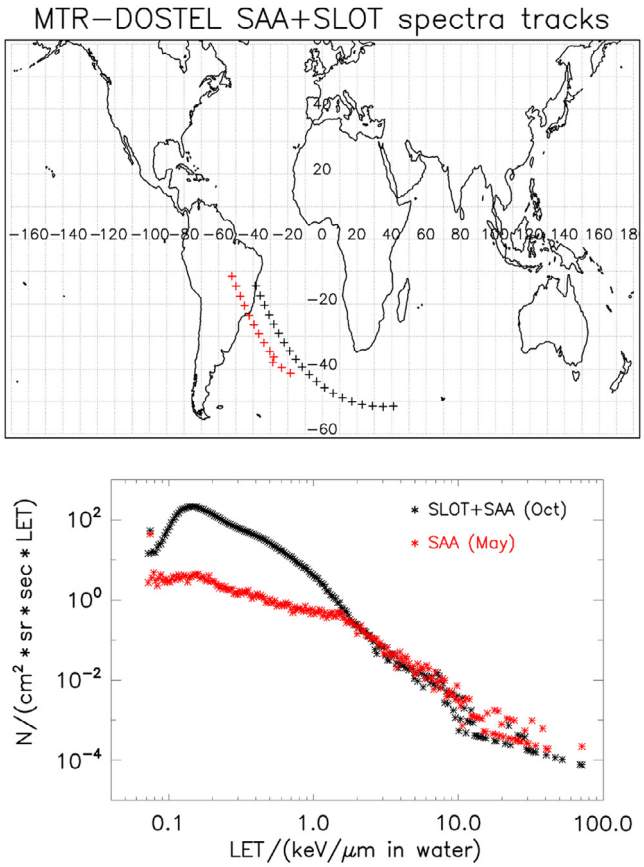

Fig. 12. The lower panel shows two LET-spectra measured by MTR-DOSTEL. In red, a spectrum of descending inner belt crossing in May 2004 is shown. The black spectrum shows the crossing of the inner belt and the EPF in September 2004. The upper panel shows the respective orbits in the same color code. An enhancement of particles with an LET below 2 keV μm^{-1}, which peaks at about 0.15 keV μm^{-1}, can be seen in the combined inner radiation belt and EPF spectrum.

be electrons. Heavier particles would have a higher rigidity and thus a larger gyro radius which leads to drift effects and efficient loss processes.

The MTR-DOSTEL measurement allows for the first time a measurement of the dose rate induced by EPF onboard ISS. The additional dose rate due to the EPF from September 24th to October 8th was calculated to be ~130 μGy day^{-1}. An evolution of this value over time could not be resolved (see Fig. 6). There are only 4 days with total coverage of EPF crossings and the geographical variations of the crossings showed higher variations than the decaying flux over time. The estimation of the total dose due to the EPF, like that measured by passive detectors, was performed by using the electron flux time profile measured by SAMPEX to scale the MTR-DOSTEL result to the whole time of the EPF presence. The electron flux in the energy range of 3.5–16 MeV was estimated from Figure 11 in 10-day intervals. Figure 13 shows the result of this procedure in the left panel. The intensity decreases from 2×10^4 (cm^2 s sr)$^{-1}$ on DOY 210 to 2×10^1 (cm^2 s sr^{-1}) on DOY 310. The fluxes were then normalized to DOY 270 (right panel of Fig. 13). On the assumption that the decay time for electron intensity on ISS altitude is the same as for SAMPEX observations, the ~130 μGy day^{-1} measured by MTR-DOSTEL around DOY 270 was then scaled to the whole time of EPF presence by using the normalized electron flux. The total normalized electron flux is proportional to the total number of electrons hitting MTR-DOSTEL (during EPF presence) in units of the amount of electrons hitting MTR-DOSTEL at DOY 270. The dose values of DOY 270 can then be scaled to the whole time of EPF presence by multiplying the dose

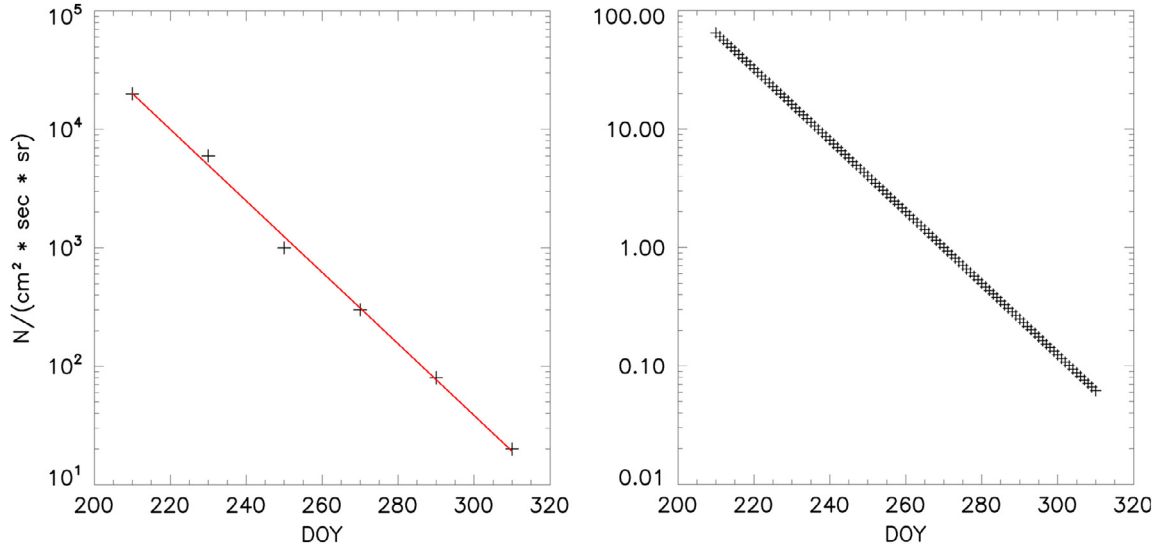

Fig. 13. Time profile of SAMPEX electron flux (3.5–16 MeV) in DOY 2004. The left panel shows a logarithmic time profile of the electron intensity at $L = 3$. A least chi-square fit through the data is shown in red. The right panel shows the fitted electron intensity normalized to DOY 270 (end of September).

value of DOY 270 with the sum of the daily normalized electron flux (see Eqs. (6) and (7)).

$$\sum_{\mathrm{DOY}} I_{e,n}(\mathrm{DOY}) = 966, \tag{6}$$

$$D_{\mathrm{EPF}} \approx 966 \times 130\ \mu\mathrm{Gy} = 125568\ \mu\mathrm{Gy}. \tag{7}$$

To compare this total absorbed dose with the results obtained with the passive detectors of MTR-1 an absorbed dose rate has to be calculated. This is done in Eq. (8). The total absorbed dose is divided by the mission time of MTR-1, which was roughly 1.5 years.

$$\dot{D}_{\mathrm{EPF}} \approx \frac{125568\ \mu\mathrm{Gy}}{365 \times 1.5\ \mathrm{days}} \approx 230 \frac{\mu\mathrm{Gy}}{\mathrm{day}}. \tag{8}$$

The resulting additional EPF induced absorbed dose rate measured with the passive MTR detectors close to MTR-DOSTEL is ~230 μGy day^{-1}. Intentional high and low estimations of the electron flux from Figure 11 resulted in 30% differences to the shown result. This can be taken as the uncertainty in the additional absorbed dose. The additional contribution to the dose rate can qualitatively explain the differences between the MTR-DOSTEL results and the ones obtained with the passive instrumentation.

5. Summary and conclusion

In this work the results obtained with MTR-DOSTEL during the MTR-1 and MTR-2B experiment phases were presented. Inside the ISS (MTR-2B) the radiation field is dominated by GCR particles, while outside the ISS (MTR-1) the trapped radiation contributes most to the radiation exposure. The comparison with the Russian DB8 detectors during the measurement inside the Zvezda module showed a good agreement of the results. The analysis of the MTR-DOSTEL data has shown that from July 2004 to November 2004 enhanced electron fluxes between $L = 2.5$ and 3.5 reached down to ISS altitudes in the region south of South Africa. This solar storm induced EPF was populated with relativistic electrons. The high flux of electrons in the EPF led to significantly higher dose values measured with the passive instrumentation of the MTR experiment, especially for the less shielded detectors like the skin detectors. That such EPFs reach down to typical altitudes of space stations was first shown by Shurshakov et al. (1996) with measurements on the Russian orbital space station MIR. The MTR-DOSTEL measurements allowed for the first time an estimation of the additional radiation exposure due to an EPF. The passive detectors close to the MTR-DOSTEL accumulated ~126 mGy from July 2004 to November 2004. This enhanced the averaged absorbed dose rate by ~230 μGy day^{-1}. The MTR-DOSTEL data indicate that the results of low shielded passive detectors (e.g. at the skin of the phantom) of MTR-1 were obtained during disturbed times of Earth's magnetosphere and do not represent the normal quite time conditions. Taking this into account MTR-DOSTEL data seems to be in good agreement with the passive detector data for the outside measurements.

Acknowledgements. This work was supported by the European commission under the FP7 project "HAMLET" GA 218817 http://www.fp7-hamlet.eu (data analysis) and by DLR under Numbers 50WB9906, 50WB0526, and 50WB0826 (hardware).

The NMDB project was supported by the European commission in the frame of FP7 under Contract No. 213007.

The editor thanks two anonymous referees for their assistance in evaluating this paper.

References

Badhwar, G., W. Atwell, G. Reitz, R. Beaujean, and W. Heinrich. Radiation measurements on the Mir Orbital Station. *Radiat. Meas.*, **35 (5)**, 393–422, 2002, DOI: 10.1016/S1350-4487(02)00072-0.

Baker, D., G. Mason, O. Figueroa, G. Colon, J. Watzin, and R. Aleman. An overview of the Solar Anomalous, and Magnetospheric Particle Explorer (SAMPEX) mission. *IEEE Trans. Geosci. Remote Sens.*, **31 (3)**, 531–541, 1993, DOI: 10.1109/36.225519.

Baker, D.N., S.G. Kanekal, X. Li, S.P. Monk, J. Goldstein, and J.L. Burch. An extreme distortion of the Van Allen belt arising from the Halloween solar storm in 2003. *Nature*, **432 (7019)**, 878–881, 2004, DOI: 10.1038/nature03116.

Beaujean, R., J. Kopp, and G. Reitz. Active dosimetry on recent space flights. *Radiat. Prot. Dosim.*, **85 (1–4)**, 223–226, 1999a.

Beaujean, R., J. Kopp, and G. Reitz. Radiation exposure in civil aircraft. *Radiat. Prot. Dosim.*, **85 (1–4)**, 287–290, 1999b.

Beaujean, R., G. Reitz, and J. Kopp. Recent European measurements inside Biorack. *Mutat. Res.*, **430 (2)**, 183–189, 1999c, DOI: 10.1016/S0027-5107(99)00129-3.

Beaujean, R., J. Kopp, S. Burmeister, F. Petersen, and G. Reitz. Dosimetry inside MIR station using a silicon detector telescope (DOSTEL). *Radiat. Meas.*, **35 (5)**, 433–438, 2002, DOI: 10.1016/S1350-4487(02)00074-4.

Berger, T., and M. Hajek. TL-efficiency – overview and experimental results over the years. *Radiat. Meas.*, **43 (26)**, 146–156, 2008, Proceedings of the 15th Solid State Dosimetry (SSD15), DOI: 10.1016/j.radmeas.2007.10.029.

Berger, T., P. Bilski, M. Hajek, M. Puchalska, and G. Reitz. The MATROSHKA experiment: results and comparison from extravehicular activity (MTR-1) and intravehicular activity (MTR-2A/2B) exposure. *Radiat. Res.*, **180 (6)**, 622–637, 2013, DOI: 10.1667/RR13148.1.

Dettmann, J., G. Reitz, and G. Gianfiglio. MATROSHKA – the first ESA external payload on the International Space Station. *Acta Astronaut.*, **60 (1)**, 17–23, 2007, DOI: 10.1016/j.actaastro.2006.04.018.

Doke, T., T. Hayashi, and T.B. Borak. Comparisons of LET distributions measured in low-earth orbit using tissue-equivalent proportional counters and the position-sensitive silicon-detector telescope (RRMD-III). *Radiat. Res.*, **156 (3)**, 310–316, 2001, DOI: 10.1667/0033-7587(2001)156[0310:COLDMI]2.0.CO;2.

Durante, M., and F.A. Cucinotta. Physical basis of radiation protection in space travel. *Rev. Mod. Phys.*, **83**, 1245–1281, 2011, DOI: 10.1103/RevModPhys.83.1245.

ICRP. The 2007 Recommendations of the International Commission on Radiological Protection. ICRP publication 103. *Ann. ICRP*, **37 (2–4)**, 2007.

ICRU. Stopping powers for electrons and protons. *Report 37*, International Commission on Radiation Units and Measurement, ICRU: Bethesda, MD, 1984.

Korth, A., and A.L. Vampola. Cross-L motion of a relativistic electron belt formed in the slot region. *J. Geophys. Res. [Space Phys.]*, **99 (A7)**, 13529–13535, 1994, DOI: 10.1029/94JA00437.

Kuznetsov, S., L. Lazutin, M. Panasyuk, L. Starostin, Y. Gotseliuk, N. Hasebe, K. Sukurai, and M. Hareyama. Solar particle dynamics during magnetic storms of July 23–27, 2004. *Adv. Space Res.*, **43 (4)**, 553–558, 2009, DOI: 10.1016/j.asr.2008.09.014.

Lishnevskii, A., M. Panasyuk, V. Benghin, V. Petrov, A. Volkov, and O. Nechayev. Variations of radiation environment onboard the ISS in the year 2008. *Cosmic Res.*, **48 (3)**, 206–210, 2010, DOI: 10.1134/S0010952510030020.

Lyons, L.R., and R.M. Thorne. Equilibrium structure of radiation belt electrons. *J. Geophys. Res.*, **78 (13)**, 2142–2149, 1973, DOI: 10.1029/JA078i013p02142.

Matthiä, D., T. Berger, and G. Reitz. Organ shielding and doses in low-earth orbit calculated for spherical and anthropomorphic phantoms. *Adv. Space Res.*, **52 (3)**, 528–535, 2013, DOI: 10.1016/j.asr.2013.03.025.

McIlwain, C.E. Coordinates for mapping the distribution of magnetically trapped particles. *J. Geophys. Res.*, **66 (11)**, 3681–3691, 1961, DOI: 10.1029/JZ066i011p03681.

Pazmandi, T., and S. Deme. Tissue dose conversion factors for protons and alpha particles in case of different detector materials, Proceedings of IRPA Regional Congress on Radiation Protection in Central Europe, September 2003, Bratislava, 2003. Published on CD-ROM ISBN 80-88806-43-7. URL: http://www.iaea.org/inis/collection/NCLCollectionStore/_Public/36/097/36097664.pdf.

Reitz, G., and T. Berger. The Matroshka facility-dose determination during An EVA. *Radiat. Prot. Dosim.*, **120 (1–4)**, 442–445, 2006, DOI: 10.1093/rpd/nci558.

Reitz, G., K. Strauch, R. Beaujean, J.K.C. Luuszik-Bhadra, and W. Heinrich. Dosimetric mapping inside BIORACK on shuttle missions STS76, STS81 and STS1984. *ESA SP1222 Biorack on Spacehab*, 161–169, 1999.

Reitz, G., R. Beaujean, E. Benton, S. Burmeister, T. Dachev, S. Deme, M. Luszik-Bhadra, and P. Olko. Space radiation measurements on-board ISS – the DOSMAP experiment. *Radiat. Prot. Dosim.*, **116 (1–4)**, 374–379, 2005, DOI: 10.1093/rpd/nci262.

Reitz, G., T. Berger, P. Bilski, R. Facius, M. Hajek, et al. Astronaut's organ doses inferred from measurements in a human phantom outside the international space station. *Radiat. Res.*, **171 (2)**, 225–235, 2009, DOI: 10.1667/RR1559.1.

Shea, M., D. Smart, and L. Gentile. Estimating cosmic ray vertical cutoff rigidities as a function of the McIlwain L-parameter for different epochs of the geomagnetic field. *Phys. Earth Planet. Inter.*, **48 (34)**, 200–205, 1987, DOI: 10.1016/0031-9201(87)90145-2.

Shurshakov, V., V. Petrov, N. Panova, Y. Ivanov, V. Makhmutov, T. Dachev, and J. Semkova. Experimental investigations of quasistable radiation belts formed after solar proton events in September–October 1989 and March 1991 based on measurements made by Liulin dosimeter-radiometer on board the MIR space station. *Adv. Space Res.*, **18 (12)**, 251–257, 1996, Proceedings of the F3.1, F3.4, F2.4 and F3.8 Symposia of {COSPAR} Scientific Commission F, DOI: 10.1016/0273-1177(96)00020-8.

Xapsos, M., P. O'Neill, and T. O'Brien. Near-Earth space radiation models. *IEEE Trans. Nucl. Sci.*, **60 (3)**, 1691–1705, 2013, DOI: 10.1109/TNS.2012.2225846.

Zhang, J., I.G. Richardson, D.F. Webb, N. Gopalswamy, E. Huttunen, et al. Solar and interplanetary sources of major geomagnetic storms (Dst $\leq$ −100 nT) during 1996–2005. *J. Geophys. Res. [Space Phys.]*, **112**, A10102, 2007, DOI: 10.1029/2007JA012321.

Zhou, D., E. Semones, D. OSullivan, N. Zapp, M. Weyland, G. Reitz, T. Berger, and E. Benton. Radiation measured for MATROSHKA-1 experiment with passive dosimeters. *Acta Astronaut.*, **66 (12)**, 301–308, 2010, DOI: 10.1016/j.actaastro.2009.06.014.

Cite this article as: Labrenz J, Burmeister S, Berger T, Heber B & Reitz G. Matroshka DOSTEL measurements onboard the International Space Station (ISS). *J. Space Weather Space Clim.*, **5**, A38, 2015, DOI: 10.1051/swsc/2015039.